4732 *Biochemistry* **2010,** *49,* 4732–4739
DOI: 10.1021/bi100007u

BIOCHEMISTRY
including biophysical chemistry & molecular biology
Article

Phosphatidylglucoside Forms Specific Lipid Domains on the Outer Leaflet of the Plasma Membrane[†]

Motohide Murate,[‡,▽] Tomohiro Hayakawa,[‡,▽,○] Kumiko Ishii,[‡] Hironori Inadome,[‡] Peter Greimel,[‡] Masaki Watanabe,[§] Yasuko Nagatsuka,[¶] Kazuki Ito,[∥] Yukishige Ito,[‡,@] Hiroshi Takahashi,[‡,⊥] Yoshio Hirabayashi,[¶,@] and Toshihide Kobayashi*[,‡,#]

[‡]*RIKEN Advanced Science Institute, Saitama, Japan,* [§]*Hitachi High-Technologies, Ibaraki, Japan,* [¶]*RIKEN Brain Science Institute, Saitama Japan,* [∥]*RIKEN Spring-8 Center, Hyogo, Japan,* [⊥]*Gunma University, Gunma, Japan,* [@]*Japan Science and Technology Agency, Saitama, Japan, and* [#]*INSERM U870, INSA-Lyon, Villeurbanne, France.* [▽]*These authors contributed equally to this work.* [○]*Present address: Advanced Materials Laboratories, Sony Corp., Tokyo, Japan.*

Received January 5, 2010; Revised Manuscript Received April 29, 2010

ABSTRACT: Phosphatidylglucoside (PtdGlc) is a recently discovered unique glycophospholipid involved in granulocytic differentiation of human promyelocytic leukemia cell line HL60 and in astrocytic differentiation in developing rodent brains. Using a PtdGlc-specific monoclonal antibody in immunofluorescence and immunoelectron microscopy, we showed that PtdGlc forms distinct lipid domains on the outer leaflet of the plasma membrane of HL60 cells and the human alveolar epithelial cell line, A549. Similar to glycosphingolipid, glucosylceramide (GlcCer), the natural form of PtdGlc exhibited a high main phase transition temperature in differential scanning calorimetry (DSC). However, unlike GlcCer, PtdGlc did not exhibit a large difference in the main phase transition temperature between the heating and cooling scans. DSC further indicated that GlcCer, but not PtdGlc, was miscible with sphingomyelin. In addition, DSC and small-angle X-ray scattering (SAXS) experiments revealed that PtdGlc was poorly miscible with phosphatidylcholine. Our results suggest that the lack of tight intermolecular interaction excludes PtdGlc from other lipid domains on the plasma membrane.

Accumulating evidence indicates that lipids are not randomly distributed in biomembranes; rather, specific lipids form lipid domains. In particular, sphingolipid-rich raftlike lipid domains have attracted a great deal of attention recently (*1*, *2*). Sphingolipid-rich domains are spontaneously formed when sphingolipids are mixed with glycerophospholipids such as phosphatidylcholine (*3*). Thus, the physical properties of the lipids play an important role in the formation of lipid domains. Although sphingolipid domains and lipid domains of synthetic phospholipids have been studied extensively, little is known about the lipid domains formed by naturally occurring phospholipids.

Phosphatidylglucoside (PtdGlc)[1] is a unique glycophospholipid originally discovered in human umbilical cord red blood cells (*4*), subsequently in human promyelocytic leukemia cell line HL60 (*5*), and in epithelial cells from various human organs (*6*) as well as in rat and mouse radial/astroglial cells (*7*, *8*). Interestingly, stimulation of HL60 cells with the Fab fragment of the monoclonal antibody against PtdGlc induced granulocyte differentiation (*5*). In contrast, stimulation with anti-ganglioside GM1 [Galβ1, 3GalNAcβ1, 4(NeuAcα2,3)Galβ1,4GlcCer] improved cell growth, whereas anti-sphingomyelin induced apoptosis of HL60 cells (*5*). PtdGlc is recovered in the Triton X-100 insoluble fraction after sucrose density gradient ultracentrifugation, suggesting that this lipid forms raftlike membrane domains (*1*, *5*). Furthermore, treatment of an immature erythroblastic leukemia cell line with a small dose of anti-PtdGlc antibody induced erythroid differentiation associated with hemoglobin production, while large-dose stimulation induced apoptosis (*9*). Finally, treatment of multipotent neural progenitor cells with anti-PtdGlc antibody was recently reported to cause epidermal growth factor receptor (EGFR) activation, suggesting that PtdGlc-enriched domains are coupled to EGFR in mediating astroglial differentiation (*8*).

Despite a growing body of evidence of the role of PtdGlc in differentiation events which may be initiated at specific lipid domains on the cell surface, little is known about its precise cellular distribution or its biophysical properties. In contrast to the structurally similar phosphatidylinositol (PtdIns), which is primarily located in the inner leaflet of the plasma membrane, immunofluorescence of HL60 cells indicated the presence of PtdGlc in the outer leaflet of the plasma membrane, where the lipids were segregated from GM1 and sphingomyelin (SM) (*5*). However, neither the detailed distribution of PtdGlc on the outer

[†]This work was supported by the RIKEN Presidential Discretionary Research Grant for Intersystem Collaboration, the Lipid Dynamics Project of RIKEN, and Grants in Aid for Scientific Research 21113530 and 22390018 (to T.K.) from the Ministry of Education, Culture, Sports, Science and Technology of Japan. H.I. was a special postdoctoral fellow of RIKEN.

*To whom correspondence should be addressed: Lipid Biology Laboratory, RIKEN Advanced Science Institute, 2-1 Hirosawa, Wako, Saitama 351-0198, Japan. Telephone: +81-48-467-9534. Fax: +81-48-467-9535. E-mail: kobayasi@riken.jp.

[1]Abbreviations: chol, cholesterol; CTxB, cholera toxin B subunit; DSC, differential scanning calorimetry; EDTA, ethylenediaminetetraacetic acid; EGFR, epidermal growth factor receptor; GalCer, galactosylceramide; GlcCer, glucosylceramide; GM1, monosialotetrahexosyl ganglioside; POPC, 1-palmitoyl-2-oleoyl-*sn*-glycero-3-phosphocholine; PtdGlc, phosphatidylglucoside; SAXS, small-angle X-ray scattering; SDS-FRL, sodium dodecyl sulfate-digested freeze fracture replica labeling; SM, sphingomyelin; TBS, Tris-buffered saline.

 Published on Web 04/30/2010

Chart 1: Structure of (a) 1-Stearoyl (C18:0)-2-arachidoyl (C20:0) *sn*-glycero-3-phospho-β-D-glucoside (phosphatidylglucoside or PtdGlc) and (b) C18:0 Glucosylceramide (GlcCer)

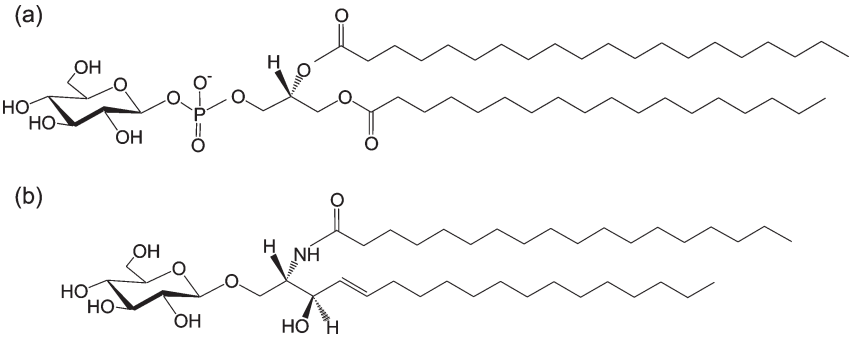

leaflet of the plasma membrane nor its distribution in the inner leaflet of the plasma membrane has been thoroughly evaluated. In this study, we examined the detailed distribution of PtdGlc on the outer as well as on the inner leaflet of the plasma membrane of HL60 cells and the human alveolar epithelial cell line, A549, using SDS-digested freeze fracture replica labeling (SDS-FRL) immunoelectron microscopy (*10*). Our results demonstrated that PtdGlc forms distinct lipid domains exclusively in the outer leaflet of the plasma membrane.

Recent biochemical studies indicate that PtdGlc exclusively exhibits a single fatty acid combination, consisting of a stearic acid (C18:0) at the *sn*-1 position and an arachidic acid (C20:0) at the *sn*-2 position of the glycerophosphate backbone (*7*) (Chart 1). In general, enrichment of saturated long-chain fatty acids is a characteristic feature of sphingolipids, like SM and glycosphingolipids. In contrast to the glucose-containing sphingolipid, glucosylceramide (GlcCer) (*11*), the physical properties of PtdGlc have not been reported. In this study, we measured the thermotropic behavior of PtdGlc for the first time and compared it with that of GlcCer. Differential scanning calorimetry (DSC) indicated that whereas GlcCer was miscible with SM, PtdGlc was not. Our results suggest that PtdGlc is excluded from sphingolipid domains because of the lack of tight intermolecular interactions with sphingolipids, leading to the formation of specific PtdGlc-rich lipid domains that could participate in cell differentiation.

MATERIALS AND METHODS

Materials. 1-Stearoyl (C18:0)-2-arachidoyl (C20:0)-*sn*-glycero-3-phospho-β-D-glucoside (phosphatidylglucoside or PtdGlc) was chemically synthesized as described previously (*12*). Mouse anti-PtdGlc monoclonal antibody DIM21 was isolated as described previously (*13*). 1-Palmitoyl (C16:0)-2-oleoyl (18:1) *sn*-glycero-3-phosphocholine (POPC), C18:0 glucosylceramide (GlcCer), and porcine brain sphingomyelin (brain SM) were obtained from Avanti Polar Lipids (Alabaster, AL). The major fatty acid composition of the brain SM was analyzed by the triple quadrupole mass spectrometer 4000Q TRAP (Applied Biosystems/MDS Sciex, Toronto, ON). The lipid samples in an acetonitrile/methanol (2:1) mixture supplemented with 0.1% ammonium formate were infused directly into the electrospray ionization (ESI) source at a flow rate of 5 μL/min with a syringe pump. Scans were run in positive ion mode over the m/z range of 300−2000. The major fatty acids in porcine brain SM were C16:0 (3%), C18:0 (34%), C18:1 (1%), C20:0 (14%), C22:0 (11%), C22:1 (5%), C24:0 (5%), C24:1 (23%), C24:2 (2%), and C26:1 (2%). Cholesterol was from Sigma (St. Louis, MO). Lysenin and anti-lysenin polyclonal (rabbit) antiserum were purchased from Peptide Institute Inc. (Osaka, Japan). Alexa 555-conjugated cholera toxin B subunit and fluorescent secondary antibodies were from Molecular Probes (Eugene, OR). HL60 cells were grown in RPMI 1640 medium supplemented with 10% fetal calf serum, 100 units/mL penicillin, and 100 μg/mL streptomycin. A549 cells were grown in DMEM containing 10% fetal calf serum, 100 units/mL penicillin, and 100 μg/mL streptomycin. PtdGlc from HL60 and A549 was identical to PtdGlc isolated from rat embryonic brain (*7*), exclusively exhibiting *sn*-1 C18:0 and *sn*-2 C20:0.

Immunofluorescence. Cells were fixed for 20 min with 3% paraformaldehyde followed by a 10 min treatment with 50 mM NH_4Cl and a 30 min treatment with 0.2% gelatin. Cells were triply labeled with DIM21, lysenin, and Alexa 555-conjugated cholera toxin B subunit. Cells were then labeled with anti-lysenin antiserum followed by Alexa 488-conjugated anti-mouse IgM and Alexa 633-conjugated anti-rabbit IgG. Specimens were observed under an LSM 510 confocal microscope equipped with a C-Apochromat 63XW Korr (1.2 NA) objective (Carl Zeiss, Oberkochen, Germany).

SDS-Digested Freeze Fracture Replica Labeling (*SDS-FRL*). SDS-digested freeze fracture immunoelectron microscopy was performed as reported previously (*10*) with some modifications. A549 cells were grown on the specimen tables for complementary replicas (Bal-Tec, Balzers, Liechtenstein) for 1 day at 37 °C. HL60 cells were collected from a culture suspension by centrifugation. Both cells were sandwiched between two specimen tables, frozen in liquid ethane cooled by liquid nitrogen, fractured in a freeze-etching machine (BAF400T, Bal-Tec) at −110 °C, and then replicated by carbon−platinum−carbon to improve the retention ratio of the membrane lipid (*14*). Replicated samples were digested in 2.5% SDS and 10% glycerin in 62.5 mM Tris buffer (pH 6.8) in the absence or presence of β-mercaptoethanol for more than 12 h at room temperature under vigorous stirring to dissolve the unfractured plasma membrane and cytoplasm. The replicas with separated membrane halves were washed in Tris-buffered saline (TBS) and labeled with biotinylated cholera toxin B subunit (Molecular Probes) and anti-PtdGlc antibody (DIM21). Biotinylated cholera toxin subunit B was detected with anti-biotin antibody conjugated to 5 nm colloidal gold (British BioCell, Cardiff, U.K.), and anti-PtdGlc antibody was detected with anti-mouse IgM antibody conjugated to 10 nm colloidal gold (British BioCell). After immunogold labeling, the replicas were washed in TBS, fixed with glutaraldehyde, washed again with pure water, and then transferred to Formvar-coated grids. Subsequently, specimens were examined under a transmission electron microscope (1200EX-II, JEOL,

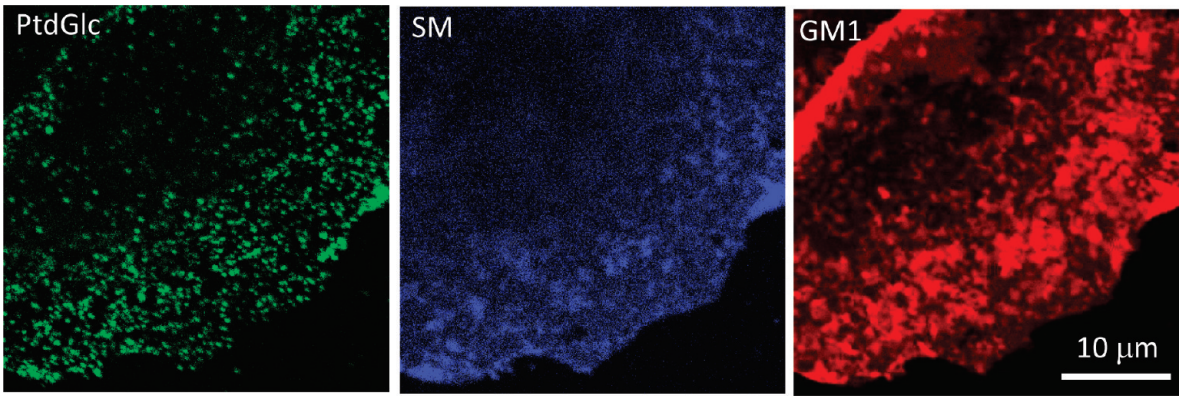

FIGURE 1: Confocal micrographs of the distribution of PtdGlc (labeled with a mouse monoclonal antibody), SM (labeled with lysenin), and GM1 (labeled with cholera toxin) in A549 cells. The cells were fixed and triply labeled as described in Materials and Methods.

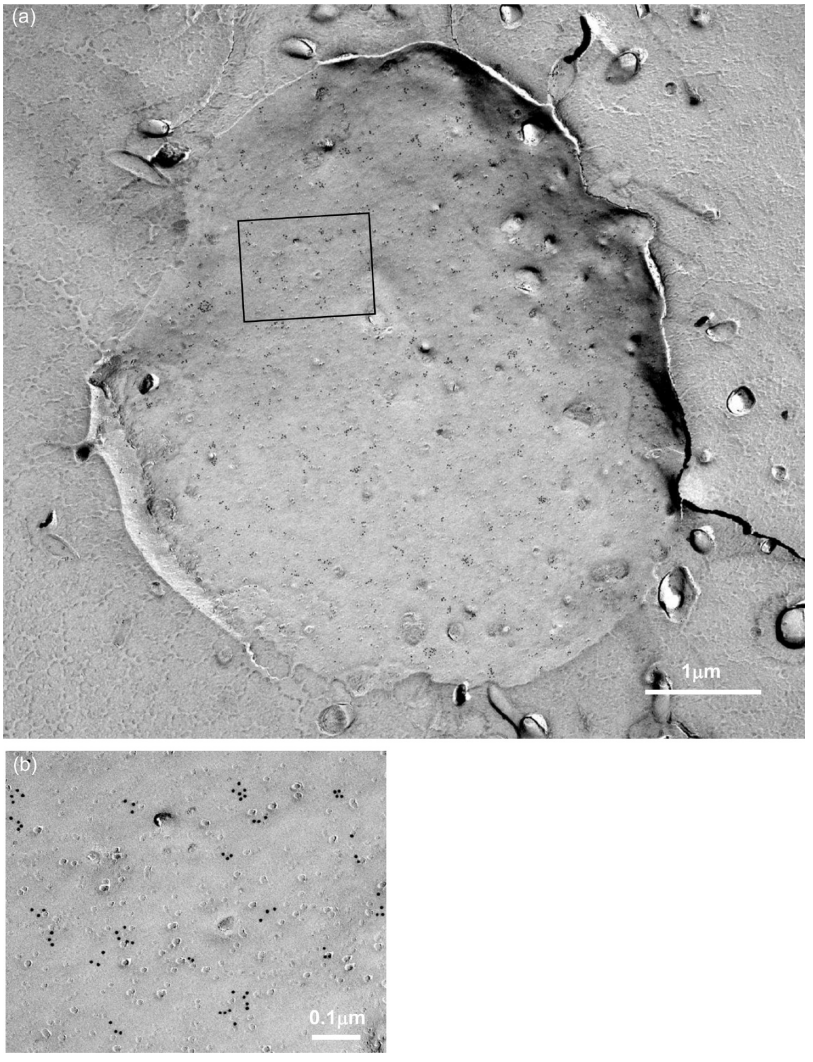

FIGURE 2: Distribution of PtdGlc on the outer leaflet of the plasma membrane of HL60 cells. A SDS-digested freeze fracture replica was prepared, and the cell surface distribution of PtdGlc was visualized with anti-PtdGlc antibody (DIM21) using 10 nm gold as described in Materials and Methods. The boxed area in panel a is magnified in panel b.

Tokyo, Japan). Electron micrographs recorded on imaging plates were scanned and digitized with an FDL 5000 imaging system (Fuji Photo Film, Tokyo, Japan). The lateral distribution of gold particles was analyzed using Ripley's K-function (*15*, *16*). Briefly, the $x-y$ coordinates of each gold particle were obtained with ImageJ and analyzed with a modified Ripley's K-function (L-function) using SPPA version 2.0 (*17*).

Differential Scanning Calorimetry (*DSC*). Stock solutions of PtdGlc and GlcCer were dissolved in a chloroform/methanol (2:1, v/v) mixture, whereas SM, POPC, and cholesterol were dissolved in chloroform. Lipid films were formed after evaporation of lipid solutions under a stream of nitrogen gas and dried under high vacuum overnight. They were hydrated and vortexed in 20 mM 4-(2-hydroxyethyl)-1-piperazineethanesulfonic

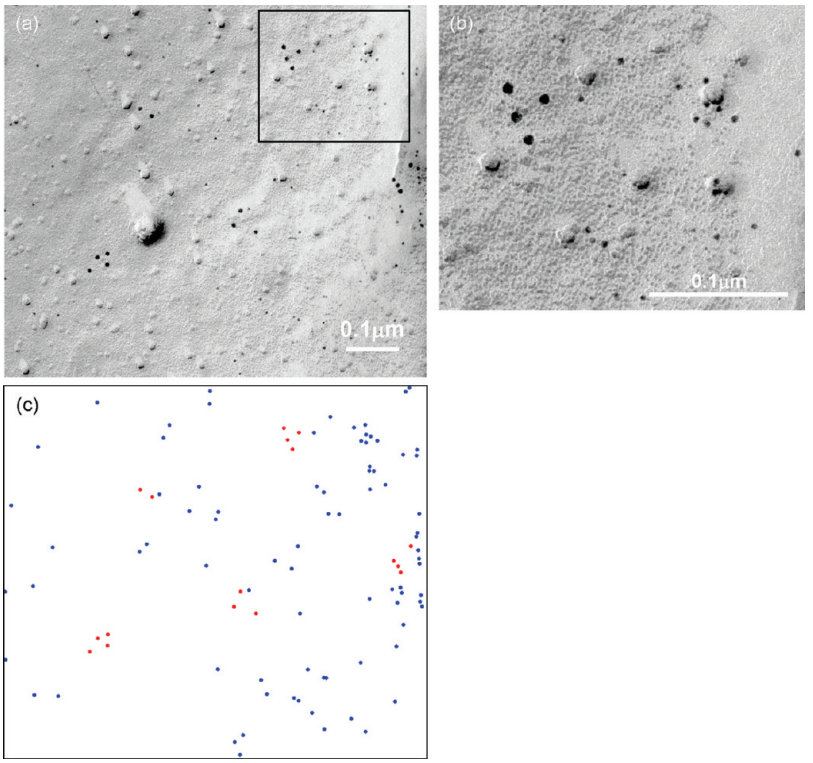

FIGURE 3: Distribution of PtdGlc (10 nm gold in panels a and b and red in panel c) and GM1 (5 nm gold in panels a and b and blue in panel c) on the outer leaflet of the plasma membrane in A549 cells. The cells were treated as described above and doubly labeled as described in Materials and Methods. The boxed area in panel a is magnified in panel b.

acid (HEPES) buffer (pH 7.0) containing 100 mM NaCl and 10 mM EDTA. The final lipid concentration was 0.5−1 mM. DSC was performed on a Microcal VP-DSC microcalorimeter (MicroCal, Northampton, MA). DSC thermograms were recorded at a scan rate of 30 °C/h for all samples. DSC scanning was performed at least 10 times, and representative data are shown in Figure 4. Sample damage after DSC measurement was checked by thin-layer chromatography. No trace of PtdGlc degradation was found under the employed experimental conditions. The obtained data were analyzed and plotted with Origin (OriginLab Corp., Northampton, MA). The transition temperature (T_m) and enthalpy (ΔH) were determined from the three-consecutive scan data of each sample.

Small-Angle X-ray Scattering (*SAXS*). The dispersed samples of PtdGlc, POPC, and the PtdGlc/POPC mixture for X-ray measurements were prepared as described for DSC measurements, with the exception that the total lipid concentration was 10 mM. To ensure homogeneous hydration of the samples, the hydrated samples in a test tube were incubated at 90 °C for at least 5 min and subsequently mildly sonicated in a water bath-type sonicator. SAXS measurements were taken at RIKEN Structural Biology Beamline I (BL45XU) at the SPring-8, 8 GeV synchrotron radiation source (Hyogo, Japan) (*18*−*20*). The X-ray wavelength used was 0.9 Å, and the beam size at the sample position was ~0.5 mm × 0.7 mm. The SAXS patterns were recorded either with a 15 s exposure by a beryllium-windowed X-ray image intensifier which is coupled with a cooled CCD camera (1000 × 1018 pixels) or with a 120 s exposure of the RIGAKU imaging plate detector (R-AXIS IV^{++}, active area size of 300 mm × 300 mm). The recorded images were corrected (*21*), and likewise, recorded buffer profiles were utilized for background subtraction. The two-dimensional scattering patterns were circularly averaged and reduced to one-dimensional profiles using FIT2D version 12.012 (http://www.esrf.fr/computing/scientific/FIT2D/), a two-dimensional data reduction and analysis program. The reciprocal spacings (s) [$s = 1/d = (2/\lambda) \sin \theta$ (where d is the lattice spacing, 2θ is the scattering angle, and λ is the X-ray wavelength)] were calibrated with silver behenate with a long period spacing of 5.838 nm (*22*).

RESULTS AND DISCUSSION

Previously, the cell surface distribution of PtdGlc was examined in HL60 cells using a human monoclonal antibody against PtdGlc (GL-2) (*5*). The GL-2 antibody exhibited a dotlike distribution throughout the cell surface. In this study, we employed the recently developed mouse monoclonal antibody against PtdGlc (DIM21), which exhibits a higher specificity than GL-2 (*7*, *13*), to investigate the cellular distribution of PtdGlc. In Figure 1, the cell surface of A549 cells was triply labeled with DIM21, lysenin [binds to SM-rich membrane domains (*16*, *23*)], and cholera toxin B subunit (CTxB) [binds to ganglioside GM1 (*24*)]. In agreement with previous results (*5*), the anti-PtdGlc antibody exhibited a dotlike distribution pattern on the cell surface. The staining pattern was different from those of lysenin and cholera toxin. Similar results were obtained with HL60 cells (data not shown).

The cellular distribution of PtdGlc was further examined using SDS-digested freeze fracture replica labeling (SDS-FRL) (*10*). For this method, plasma membranes were split into two monolayers and cast in platinum and carbon at low temperatures. Subsequent treatment with SDS held lipids on the metal surface, enabling the labeling of these lipids with antibodies. A big advantage of this method is the ability to label the lipids of the outer and inner leaflet, separately. Figure 2 shows the outer leaflet of the plasma membrane of HL60 cells. The distribution of PtdGlc was studied with the DIM21 antibody, followed by an

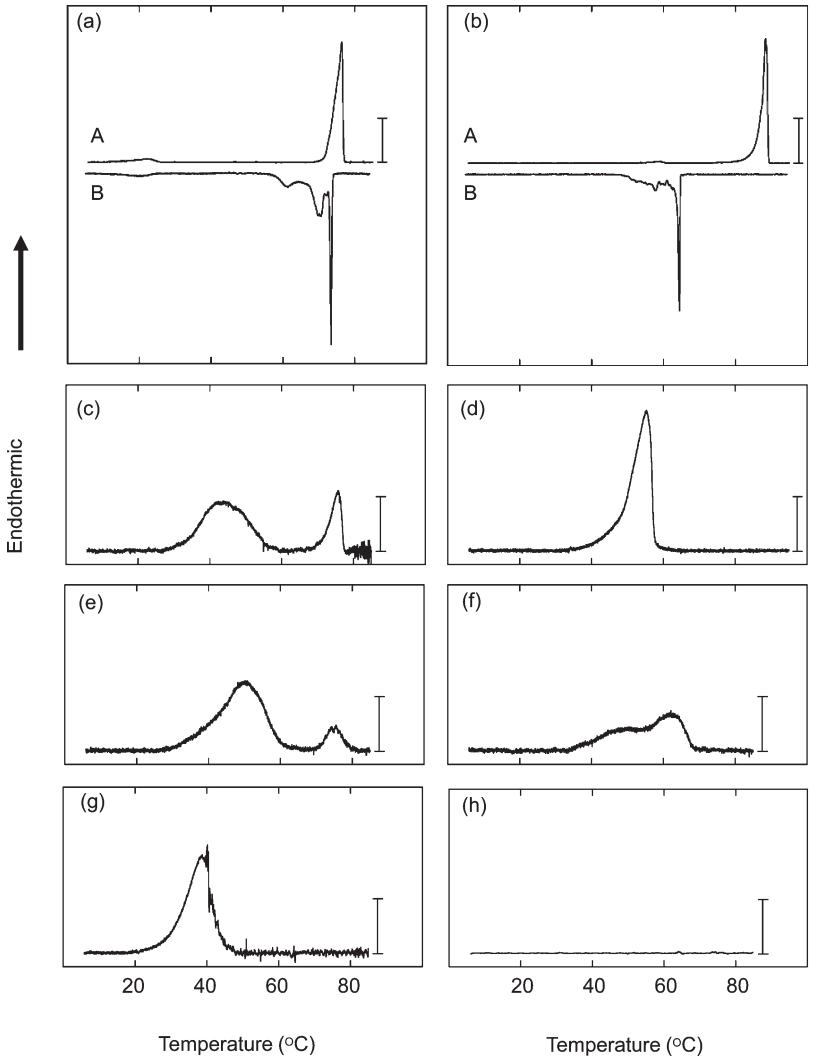

FIGURE 4: DSC thermograms of PtdGlc (a), GlcCer (b), a PtdGlc/brain SM mixture (1:1 molar ratio) (c), a GlcCer/brain SM mixture (1:1 molar ratio) (d), a PtdGlc/brain SM/cholesterol mixture (1:1:1 molar ratio) (e), a PtdGlc/POPC mixture (1:1 molar ratio) (f), brain SM (g), and POPC (h). Data were normalized with respect to the total mass of lipids (in panel d, cholesterol was not included to calculate the lipid mass). In panels a and b, A and B indicate the thermograms of heating and cooling, respectively. The vertical scale bars in panels a and b and panels c−h are 2 and 0.4 kcal mol^{-1} $°C^{-1}$, respectively.

anti-mouse IgM antibody conjugated with 10 nm gold. Consistent with the immunofluorescence results, immunogold staining was not evenly distributed. Instead, distinct clusters of immunogold were observed throughout the membrane. In Figure 3, the outer leaflet of the plasma membrane of A549 cells was doubly labeled with DIM21 and CTxB. The distribution of DIM21 and CTxB was marked with different sized colloidal gold particles. In Figure 3c, 10 nm gold (marking DIM21) was colored red whereas 5 nm gold (marking CTxB) was colored blue. Figure 3 indicates that PtdGlc forms distinct lipid domains in the outer leaflet of the plasma membrane of A549 cells and these domains do not overlap with the distribution of GM1. We then compared the distribution of PtdGlc between the outer leaflet and the inner leaflet of the plasma membrane. In HL60 cells, the number of immunogold particles on the outer leaflet was 110.2 ± 51.4 per square micrometer (n = 17), whereas on the inner leaflet, this number was 2.3 ± 3.4 per square micrometer (n = 16). In A549, the outer leaflet exhibited a density of 22.1 ± 29.1 particles/μm^2 (n = 11) and the inner leaflet gave 0.75 ± 0.9 particle/μm^2 (n = 18). The larger deviation in the outer leaflet of A549 cells was possibly due to the lower density of PtdGlc in these cells. Our results indicate that PtdGlc is almost exclusively distributed in the outer leaflet of the plasma membrane in HL60 and A549 cells. The lateral distribution of PtdGlc in the membrane was analyzed using Ripley's K-function (*16*, *25*). K-Function analysis indicated that PtdGlc forms domains whose radius was 48.2 ± 5.4 nm (n = 17) in HL60 cells and 68.9 ± 27.2 nm (n = 11) in A549 cells.

To understand the molecular mechanisms that lead to the formation of PtdGlc domains, we studied the physical properties of synthetic PtdGlc (*12*). Figure 4a shows the DSC thermograms of synthetic PtdGlc. Dispersed PtdGlc underwent a low-enthalpy endothermic transition at 23.73 ± 0.57 °C (ΔH = 0.97 ± 0.04 kcal/mol). Further heating resulted in the high-temperature, high-enthalpy endothermic transition at 76.42 ± 0.05 °C (ΔH = 14.19 ± 0.13 kcal/mol) characteristic of chain melting. Upon cooling, PtdGlc exhibited supercooling. In addition to the sharp transition at 73.47 ± 0.05 °C, two additional distinct exothermic peaks at ~70.0 and ~61.5 °C have been observed. The total enthalpy under this complex exotherm between 55 and 74 °C was essentially identical to that of the endothermic chain melting transition observed upon heating (ΔH = 14.53 ± 0.12 kcal/mol). As observed in the heating scan, a low-enthalpy exothermic transition occurred at 20.68 ± 0.12 °C upon cooling (ΔH = 0.84 ± 0.04 kcal/mol). After the sample had cooled to 5 °C, immediate

reheating resulted in a heating scan identical to that shown in Figure 4a.

A high gel-to-liquid crystalline phase transition temperature has been reported in glycosphingolipids such as glucosylceramide (GlcCer) (*11*). C16:0-GlcCer exhibits a chain melting transition of ~87 °C (*11*). In this study, we measured the thermotropic behavior of C18:0-GlcCer, which is one of the major molecular species of GlcCer in neuronal cells (*26*) and structurally close to PtdGlc. C18:0-GlcCer exhibited a slightly higher chain melting transition than C16:0-GlcCer at 88.50 ± 0.16 °C (ΔH = 11.79 ± 0.16 kcal/mol) (Figure 4b). In addition to the major transition, C18:0-GlcCer underwent a broad, low-enthalpy endothermic transition at 58.70 ± 0.59 °C (ΔH = 0.32 ± 0.05 kcal/mol). Similar to PtdGlc, C16:0-GlcCer, C16:0-galactosylceramide (C16:0-GalCer) (*11*), and C18:0-GlcCer (Figure 4b) exhibited complex exotherms on cooling (T_m and ΔH of 64.31 ± 0.13 °C and 9.32 ± 0.18 kcal/mol, respectively, in Figure 4b). The difference in the main phase transition temperature between heating and cooling was dramatically different between PtdGlc and GlcCer. While C16:0-GalCer exhibited a difference of ~23 °C, C16:0-GlcCer a difference of ~20 °C (*11*), and C18:0-GlcCer a difference of ~24 °C (Figure 4b), PtdGlc exhibited a difference of only ~3 °C (Figure 4a). The difference between the heating and cooling scan in the case of C16:0-GlcCer and C16:0-GalCer has been attributed to the formation of a metastable phase (*11*). On the basis of the transition enthalpy characteristics of PtdGlc, no metastable phase was formed below ~55 °C. In contrast, the broad, low-enthalpy endothermic transition of C18:0-GlcCer at ~59 °C indicates the presence of the metastable phase.

It has been suggested that the very high phase transition temperature of GlcCer and GalCer is caused by both a highly ordered chain packing mode and a lateral intermolecular hydrogen bonding network involving the sphingosine backbone, the sugar group, and the interbilayer water molecules (*27*). Consequently, our results suggest that PtdGlc does not exhibit similarly tight intermolecular interaction as observed in glycosphingolipids, possibly due to the presence of the diacylglycerol backbone in combination with the relatively large headgroup of PtdGlc, containing a negatively charged phosphate group.

Previous DSC studies revealed that GalCer is miscible with SM (*28*). To examine the possibility that the formation of distinct lipid domains of PtdGlc is due to the immiscibility of this lipid with other plasma membrane lipids, we decided to conduct a DSC study with a mixture of PtdGlc and brain SM as well as C18:0-GlcCer and brain SM. During the heating scan of the mixture of PtdGlc and brain SM (1:1), two distinct endothermic peaks at 45.15 ± 1.37 °C (ΔH = 5.33 ± 0.26 kcal/mol) and 75.53 ± 0.41 °C (ΔH = 1.85 ± 0.19 kcal/mol) were detected (Figure 4c). Since unmixed samples of brain SM and PtdGlc exhibited distinct chain melting phase transitions at 38.52 ± 0.09 °C (ΔH = 6.00 ± 0.55 kcal/mol) (Figure 4g) and 76.42 ± 0.05 °C (Figure 4a) correspondingly, it is conceivable that the two endothermic transitions in Figure 4c are mainly composed of brain SM and PtdGlc, respectively. Consequently, this result indicates that brain SM and PtdGlc tend to retain separate phases. However, the peak temperatures in Figure 4c are shifted from the chain melting temperature of brain SM and PtdGlc, and a broad shoulder appeared at ~52 °C, indicating partial miscibility of PtdGlc and brain SM. The thermogram of the cooling scan was essentially the same as that of the heating scan (data not shown). In contrast, the heating scan of the mixture of C18:0-GlcCer and brain SM (1:1) showed a single transition peak centered at 55.23 ± 0.11 °C (ΔH = 7.37 ± 0.13 kcal/mol) (Figure 4d), while the original chain melting endothermic peaks of brain SM and C18:0-GlcCer disappeared, indicating that C18:0-GlcCer and brain SM are fairly miscible. Recent computational simulation of SM molecules indicated that the OH group of the molecule in the sphingosine moiety is the main donor for intramolecular hydrogen bonds, whereas the NH group is the dominating donor in the case of intermolecular hydrogen bonds between lipids (*29*). The NH group primarily binds to the hydroxyl oxygens of other SMs, as well as to a varying extent to a carbonyl or other oxygens. GlcCer shares both features, the NH group and the OH group, with SM, in contrast to PtdGlc, which is lacking both groups. This structural difference might be the reason for the different miscibility of PtdGlc and GlcCer with brain SM.

We next examined the effect of cholesterol on the miscibility of PtdGlc and brain SM. The thermogram of the PtdGlc/brain SM/chol (1:1:1 molar ratio) mixture (Figure 4e) exhibited two broad but distinct endothermic transitions, at 49.79 ± 1.16 °C (ΔH = 5.25 ± 0.28 kcal/mol) and 74.71 ± 4.76 °C (ΔH = 0.71 ± 0.21 kcal/mol), in the range of 5−95 °C. This transition profile is similar to the thermogram of the PtdGlc/brain SM mixture (Figure 4c). Hence, it is conceivable that the low-temperature transition (~50 °C) originates from brain SM while the high-temperature transition (~75 °C) stems from PtdGlc. However, compared to that of the PtdGlc/brain SM mixture (Figure 4c), the low-temperature transition peak was shifted to a higher temperature (~45 to ~50 °C) while the peak at ~75 °C became smaller. These results indicate that cholesterol induces the mixing of PtdGlc and brain SM, but even with a high cholesterol content, full miscibility is not achieved.

We also investigated the miscibility of PtdGlc and POPC, another abundant component of the plasma membrane. Figure 4f shows the DSC thermogram of the PtdGlc/POPC (1:1 molar ratio) mixture. The characteristic phase transition peak of PtdGlc (at ~75 °C) disappeared, and a broad endothermic transition peak at 63.21 ± 1.54 °C with a low-temperature shoulder (at ~50 °C) was observed between ~30 and ~70 °C. The ΔH in this broad endotherm between 30 and 70 °C was 6.04 ± 0.13 kcal/mol. Since POPC itself did not exhibit a transition peak over the examined temperature range (5−95 °C) (Figure 4h), it is reasonable that the observed broad peak with a shoulder was mainly derived from the transition of PtdGlc. In addition, such a broad two-peak transition suggests that PtdGlc was distributed heterogeneously.

To further clarify the phase separation of a PtdGlc/POPC mixture, SAXS measurements were performed. Figure 5 shows the SAXS profile of PtdGlc, POPC, and a PtdGlc/POPC (1:1 molar ratio) mixture at 25 °C. PtdGlc exhibited three reflection peaks in the small-angle region over the broad scattering of the form factor (Figure 5a). These reflections correspond well with first- to third-order lamellar reflections with a 10.21 nm lamellar distance (*d*-spacing). POPC also exhibited lamellar structure with a *d*-spacing of 6.25 nm (Figure 5b). The PtdGlc/POPC mixture exhibited several reflections in the small-angle region (Figure 5c). The peak positions of these reflections indicate the presence of two lamellar structures with *d*-spacings of 9.28 and 6.58 nm, thus exhibiting a clear phase separation of two lamellar phases. Comparison of this reflection profile and *d*-spacing with the previously discussed SAXS data of PtdGlc (Figure 5a) and POPC (Figure 5b) indicates that the two observed lamellar structures (Figure 5c) can be attributed to phase-separated PtdGlc- and POPC-rich regions.

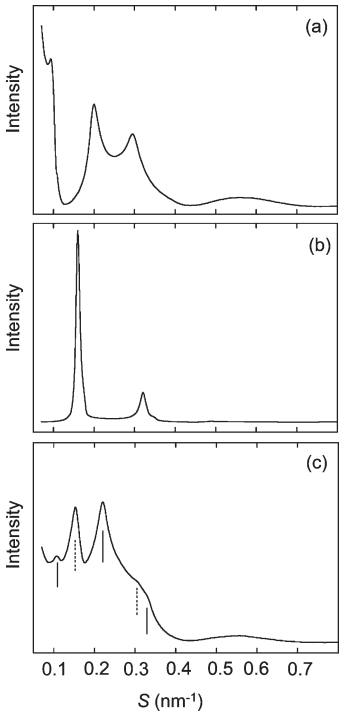

FIGURE 5: Small-angle X-ray scattering profiles of dispersed PtdGlc (a), POPC (b), and a PtdGlc/POPC mixture (c) in 20 mM HEPES buffer (pH 7.0), containing 100 mM NaCl and 10 mM EDTA at 25 °C. Bold and dashed vertical lines in panel c indicate the positions of lamellar peaks that originated from 9.28 and 6.58 nm lamellar distances (*d*-spacing), respectively.

Although the characteristic main phase transition peak of PtdGlc, as observed in the PtdGlc/SM (Figure 4c) and PtdGlc/SM/chol (Figure 4e) mixtures, was not present in the thermogram of the PtdGlc/POPC (Figure 4f) mixtures, SAXS data strongly indicate that PtdGlc and POPC are not well miscible under our experimental conditions. However, the *d*-spacing in the PtdGlc/POPC mixture of the PtdGlc-rich region (9.28 nm) was significantly smaller than that of pure PtdGlc (10.21 nm), while the POPC-rich region (6.58 nm) was larger than that of pure POPC (6.25 nm), indicating that certain amounts of both components were mixed with each other.

In this study, we showed that PtdGlc forms distinct lipid domains on the outer leaflet of the plasma membrane in HL60 and A549 cells. Our DSC and SAXS studies suggest that this is due to the immiscibility of PtdGlc with the other lipids of the outer leaflet, mainly sphingolipids (SM) and glycerolipids (POPC). Moreover, even in the presence of cholesterol, PtdGlc was phase separated from SM. PtdGlc is thought to be involved in granulocytic differentiation of HL60 cells (*5*, *30*) as well as in astrocytic differentiation in developing rodent brains (*8*, *30*). Our results, in combination with these observations, suggest that physically segregated PtdGlc domains might provide a unique lipid environment for these signaling processes.

ACKNOWLEDGMENT

We are grateful to Françoise Hullin-Matsuda for critically reading the manuscript.

REFERENCES

1. Lingwood, D., Kaiser, H. J., Levental, I., and Simons, K. (2009) Lipid rafts as functional heterogeneity in cell membranes. *Biochem. Soc. Trans. 37*, 955–960.
2. Jacobson, K., Mouritsen, O. G., and Anderson, R. G. (2007) Lipid rafts: At a crossroads between cell biology and physics. *Nat. Cell Biol. 9*, 7–14.
3. London, E. (2005) How principles of domain formation in model membranes may explain ambiguities concerning lipid raft formation in cells. *Biochim. Biophys. Acta 1746*, 203–220.
4. Nagatsuka, Y., Kasama, T., Ohashi, Y., Uzawa, J., Ono, Y., Shimizu, K., and Hirabayashi, Y. (2001) A new phosphoglycerolipid, 'phosphatidylglucose', found in human cord red cells by multi-reactive monoclonal anti-i cold agglutinin, mAb GL-1/GL-2. *FEBS Lett. 497*, 141–147.
5. Nagatsuka, Y., Hara-Yokoyama, M., Kasama, T., Takekoshi, M., Maeda, F., Ihara, S., Fujiwara, S., Ohshima, E., Ishii, K., Kobayashi, T., Shimizu, K., and Hirabayashi, Y. (2003) Carbohydrate-dependent signaling from the phosphatidylglucoside-based microdomain induces granulocytic differentiation of HL60 cells. *Proc. Natl. Acad. Sci. U.S.A. 100*, 7454–7459.
6. Kitamura, Y., Okazaki, T., Nagatsuka, Y., Hirabayashi, Y., Kato, S., and Hayashi, K. (2007) Immunohistochemical distribution of phosphatidylglucoside using anti-phosphatidylglucoside monoclonal antibody (DIM21). *Biochem. Biophys. Res. Commun. 362*, 252–255.
7. Nagatsuka, Y., Horibata, Y., Yamazaki, Y., Kinoshita, M., Shinoda, Y., Hashikawa, T., Koshino, H., Nakamura, T., and Hirabayashi, Y. (2006) Phosphatidylglucoside exists as a single molecular species with saturated fatty acyl chains in developing astroglial membranes. *Biochemistry 45*, 8742–8750.
8. Kinoshita, M. O., Furuya, S., Ito, S., Shinoda, Y., Yamazaki, Y., Greimel, P., Ito, Y., Hashikawa, T., Machida, T., Nagatsuka, Y., and Hirabayashi, Y. (2009) Lipid rafts enriched in phosphatidylglucoside direct astroglial differentiation by regulating tyrosine kinase activity of epidermal growth factor receptors. *Biochem. J. 419*, 565–575.
9. Kawano-Yamamoto, C., Muroi, K., Nagatsuka, Y., Higuchi, M., Kikuchi, S., Nagai, T., Hakomori, S. I., and Ozawa, K. (2006) Establishment and characterization of a new erythroblastic leukemia cell line, EEB: Phosphatidylglucoside-mediated erythroid differentiation and apoptosis. *Leuk. Res. 30*, 829–839.
10. Fujimoto, K., Umeda, M., and Fujimoto, T. (1996) Transmembrane phospholipid distribution revealed by freeze-fracture replica labeling. *J. Cell Sci. 109*, 2453–2460.
11. Saxena, K., Duclos, R. I., Zimmermann, P., Schmidt, R. R., and Shipley, G. G. (1999) Structure and properties of totally synthetic galacto- and gluco-cerebrosides. *J. Lipid Res. 40*, 839–849.
12. Greimel, P., and Ito, Y. (2008) First synthesis of phosphatidyl-β-D-glucoside. *Tetrahedron Lett. 49*, 3562–3566.
13. Yamazaki, Y., Nagatsuka, Y., Oshima, E., Suzuki, Y., Hirabayashi, Y., and Hashikawa, T. (2006) Comprehensive analysis of monoclonal antibodies against detergent-insoluble membrane/lipid rafts of HL60 cells. *J. Immunol. Methods 311*, 106–116.
14. Fujita, A., and Fujimoto, T. (2007) Quantitative retention of membrane lipids in the freeze-fracture replica. *Histochem. Cell Biol. 128*, 385–389.
15. Ripley, B. D. (1979) Tests of randomness for spatial point patterns. *J. R. Stat. Soc. Ser B 41*, 368–374.
16. Kiyokawa, E., Baba, T., Otsuka, N., Makino, A., Ohno, S., and Kobayashi, T. (2005) Spatial and functional heterogeneity of sphingolipid-rich membrane domains. *J. Biol. Chem. 280*, 24072–24084.
17. Hasse, P. (1995) Spatial pattern analysis in ecology based on Ripley's K-function: Introduction and methods for edge correction. *Journal of Vegetation Science 6*, 575–582.
18. Fujisawa, T., Inoue, K., Oka, T., Iwamoto, H., Uraga, T., Kumasaka, T., Inoko, Y., Yagi, N., Yamamoto, M., and Ueki, T. (2000) Small-angle X-ray scattering station at the SPring-8 RIKEN beamline. *J. Appl. Crystallogr. 33*, 797–800.
19. Hayakawa, T., Makino, A., Murate, M., Sugimoto, I., Hashimoto, Y., Takahashi, H., Ito, K., Fujisawa, T., Matsuo, H., and Kobayashi, T. (2007) pH-dependent formation of membranous cytoplasmic body-like structure of ganglioside GM1/bis(monoacylglycero)phosphate mixed membranes. *Biophys. J. 92*, L13–L16.
20. Iwamoto, K., Hayakawa, T., Murate, M., Makino, A., Ito, K., Fujisawa, T., and Kobayashi, T. (2007) Curvature-dependent recognition of ethanolamine phospholipids by duramycin and cinnamycin. *Biophys. J. 93*, 1608–1619.
21. Ito, K., Kamikubo, H., Yagi, N., and Amemiya, Y. (2005) Correction method and software for image distortion and nonuniform response in charge-coupled device-based X-ray detectors utilizing X-ray image intensifier. *Jpn. J. Appl. Phys. 44*, 8684–8691.
22. Huang, T., Toraya, H., Blanton, T., and Wu, Y. (1993) X-ray powder diffraction analysis of silver behenate, a possible low-angle diffraction standard. *J. Appl. Crystallogr. 26*, 180–184.

23. Ishitsuka, R., Yamaji-Hasegawa, A., Makino, A., Hirabayashi, Y., and Kobayashi, T. (2004) A lipid-specific toxin reveals heterogeneity of sphingomyelin-containing membranes. *Biophys. J. 86*, 296–307.
24. De Haan, L., and Hirst, T. R. (2004) Cholera toxin: A paradigm for multi-functional engagement of cellular mechanisms. *Mol. Membr. Biol. 21*, 77–92.
25. Prior, I. A., Muncke, C., Parton, R. G., and Hancock, J. F. (2003) Direct visualization of Ras proteins in spatially distinct cell surface microdomains. *J. Cell Biol. 160*, 165–170.
26. Robert, J., Rebel, G., and Mandel, P. (1977) Glycosphingolipids from cultured astroblasts. *J. Lipid Res. 18*, 517–522.
27. Freire, E., Bach, D., Correa-Freire, M., Miller, I., and Barenholz, Y. (1980) Calorimetric investigation of the complex phase behavior of glucocerebroside dispersions. *Biochemistry 19*, 3662–3665.
28. Johnston, D. S., and Chapman, D. (1988) A calorimetric study of the thermotropic behaviour of mixtures of brain cerebrosides with other brain lipids. *Biochim. Biophys. Acta 939*, 603–614.
29. Mombelli, E., Morris, R., Taylor, W., and Fraternali, F. (2003) Hydrogen-bonding propensities of sphingomyelin in solution and in a bilayer assembly: A molecular dynamics study. *Biophys. J. 84*, 1507–1517.
30. Nagatsuka, Y., and Hirabayashi, Y. (2008) Phosphatidylglucoside: A new marker for lipid rafts. *Biochim. Biophys. Acta 1780*, 405–409.